Cooperative self-assembly of dimer junctions driven by π-stacking leads to conductance enhancement

Xiaoyun Pan[1+], Enrique Montes[2+], Wudmir Y. Rojas[2], Brent Lawson[3], Héctor Vázquez[2], Maria Kamenetska[1,3,4]**

[+]equal contributions

*corresponding authors

AUTHOR ADDRESS.

[1]Department of Chemistry, Boston University, Boston MA, 02155

[2]Institute of Physics, Czech Academy of Sciences, Cukrovarnická 10, Prague, CZ-162 00 Czech Republic

[3]Department of Physics, Boston University, Boston MA, 02155

[4]Division of Material Science and Engineering; Boston University, Boston MA, 02155

KEYWORDS: Electrical conductivity, π-stacking, In situ assembly, Intermolecular interaction, Benzimidazole, single molecule conductance, metal-organic interface

ABSTRACT: We demonstrate enhanced electronic transport through dimer molecular junctions which self-assemble between two gold electrodes in π-π stabilized binding configurations. Single molecule junction conductance measurements show that benzimidazole molecules assemble into dimer junctions with a per-molecule conductance that is higher than in monomer junctions. Density functional theory calculations reveal that parallel stacking of two benzimidazoles between electrodes is the most energetically favorable due to the large π system. Imidazole is smaller and has greater conformational freedom to access different stacking angles. Transport calculations confirm that the conductance enhancement of benzimidazole dimers results from the changed binding geometry of dimers on gold which is stabilized and made energetically accessible by intermolecular π-stacking. We engineer imidazole derivatives with higher monomer conductance than benzimidazole and large intermolecular interaction that promote cooperative *in situ* assembly of more transparent dimer junctions and suggest at the potential of molecular devices based on self-assembled molecular layers.

TEXT: Creating conductive and tunable single molecule devices remains the long-term challenge of molecular electronics.[1–3] Efforts to engineer the electronic structure of molecular junctions have focused on leveraging synthetic control to create molecules with desired functionality.[3–6] Typically,

molecules with pre-designed components are synthesized and then introduced into the junction, where they can bridge two electrodes through a pair of substituent linker groups.[4]

An alternative approach is to design molecular components which can rearrange and self-assemble into novel molecular structures in the junction.[7–9] For example, imidazole (Im)—a conjugated five-member heterocycle—can become deprotonated to imidazolate in the junction environment and then bridge gold electrodes to form Im-gold bridges.[8,10–12] Other work shows that intermolecular interactions can be harnessed to create new junction structures.[13–15] For example, researchers have synthetically manipulated π–π coupling between oligo-phenylene-ethynylene (OPE) molecules to achieve junctions with through-space transport,[16] quantum interference,[17] and environmental controls.[18] Additionally, other conjugated molecules containing multiple π-π stacked units were observed to demonstrate a significant increase in conductance due to constructive quantum interference.[17,19]

Here, we demonstrate that intermolecular van der Waals interactions like π-π stacking can drive cooperative binding of several molecules between metal electrodes and promote the formation of molecular dimer junctions with enhanced conductance per molecular unit. We show that benzimidazole (BI), a larger heterocycle containing an Im fused to a benzene shown in Figure 1a, assembles to bridge two gold electrodes upon deprotonation just like the Im in Figure 1b reported previously. Unlike Im, BI creates junction structures with multiple conductance peaks which are *not* integer multiples of a monomer junction, but display a higher conductance per molecule. Density Functional Theory (DFT) calculations show that van der Waals intermolecular interactions between the aromatic BI molecules stabilize the π-π stacked BI dimers over other molecular arrangements in the junction and that intermolecular binding energy is ~20 times k_BT. In contrast, the Im dimer binding energy is much less sensitive to relative orientation between the molecules. Transport calculations show that energetically preferred BI dimer junctions are stabilized by intermolecular interactions in a junction conformation with higher conductances per molecule than monomer junctions. We demonstrate how we can tune this cooperativity effect and overall junction conductance through synthetic substitution of Im derivatives by designing a phenyl-substituted Im with increased intermolecular interactions which assemble into more transparent dimer junctions than either BI or Im. Overall, this work demonstrates a new self-

assembly approach which leverages intermolecular interactions to achieve molecular junctions with improved electronic properties.

We perform Scanning Tunneling Microscope Break Junction (STMBJ) measurements using a home-built setup as previously described.[20–22] Briefly, we bring two gold electrodes into contact and then record a conductance trace while the electrodes are retracted under constant bias. Sample traces are shown in Figure S1a. 2D histograms constructed out of at least 5000 such traces collected in the presence of BI and Im without data selection are shown in Figure 1a and b respectively.[23] By binning the conductance only, we obtain 1D histograms, shown in Figure 1c, where molecular signatures appear as distinct conductance peaks.

We note that the conductance signatures observed for BI are similar to those of Im, published previously.[8,10] In earlier work, the low conductance peaks (LG) have been attributed to *in situ* assembly of extended structures in the junction.[8,10] In this work, we focus on the high conductance region (HG) boxed in green in Figure 1a-c. Several distinct features labeled as G1-3 are present both in the Im and BI histograms in the HG region. We observe that the length of these features in the 2D histograms (Figures 1a-b) is very similar for both molecules and strongly suggests identical binding geometries are responsible for formation of these molecular junctions with BI and Im.

In addition, we observe that BI only forms junctions in neutral to basic conditions, as has also been previously reported for Im.[8,11,24] This result indicates that deprotonation of the BI at the nitrogen linkers is required for junction formation. The similarity of pH-dependent conductance signatures for BI and Im establishes that the same binding mechanism is responsible for the HG peaks of both molecules. We conclude that BI bridges the gold electrodes by binding through the nitrogen lone-pairs of deprotonated molecules as has been previously found for Im. The HG conductance signals from Im and BI are attributed to monomer (G1), dimer (G2), and trimer (G3) junction formations.

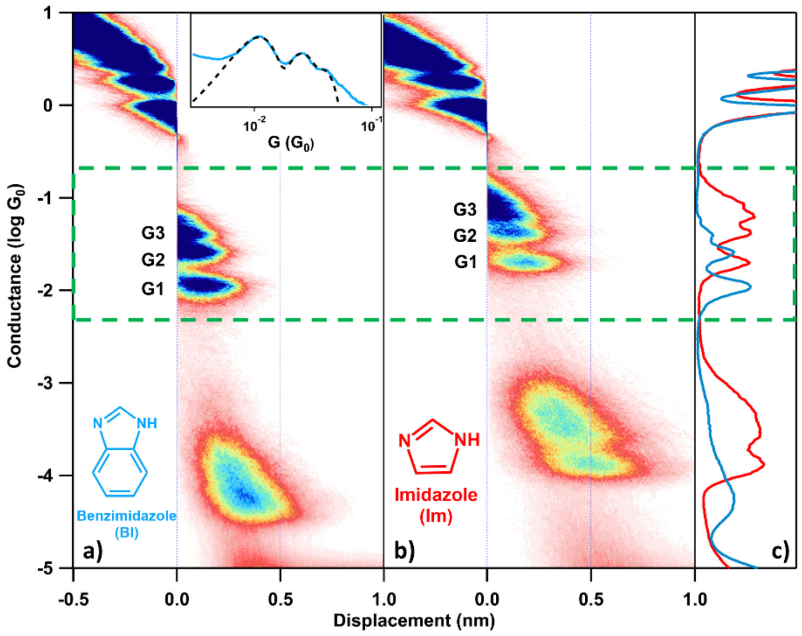

Figure 1. a) 2D histogram of benzimidazole.Top inset: We fit the 1D histograms with a sum of three Gaussian fits to obtain G1-3 conductance values for BI. Bottom inset:Chemical structure of benzimidazole. b) 2D histogram of imidazole; inset: chemical structure of imidazole. c) 1D histogram of benzimidazole (blue) and imidazole (red). Green dash box contains the conductance region of interest in this work.

	G1 (G_0)	G2 (G_0)	G2/G1		G1 (G_0)	G2 (G_0)	G2/G1
Im	1.96×10^{-2}	4.08×10^{-2}	2.08	BI	1.14×10^{-2}	2.62×10^{-2}	2.30
2MeIm	1.97×10^{-2}	4.36×10^{-2}	2.21	2MeBI	1.31×10^{-2}	2.94×10^{-2}	2.24
2PhIm	2.07×10^{-2}	4.94×10^{-2}	2.38	2PhBI	1.30×10^{-2}	2.79×10^{-2}	2.16

Table 1. List of measured conductance histogram peak values and their ratios of molecules studied. Each entry in Table 1 is an average of at least 4 experiments conducted on different days with a minimum of 5000 traces collected per experiment. The standard error is less than 1%， and the day to day variation in G1-3 peak positions is less than 3% (see SI Table S1 for details).

We fit the 1D histograms with a sum of three Gaussian fits to obtain G1-3 conductance values for BI. Results from four experiments are averaged and summarized in Table 1. Im fitting results using a similar protocol have been published previously and are reproduced in Table 1.[8] Interestingly, we observe that the conductance of the monomer peak (G1), is lower for BI than for

Im; we measure 1.1×10^{-2} G_0 and 2.0×10^{-2} G_0, for BI and Im respectively. G2 peaks of Im junctions occur at multiples of the Im G1 conductance value, which is expected for molecules binding in parallel to create two uncoupled conductance channels. This is reflected in the G2/G1 conductance ratio for Im junctions which is ~2 in Table 1. Notably, in BI junctions, comparing the conductance of G1 and G2 peaks, we observe a ratio G2/G1 equaling 2.3. These results indicate that the conductance of 2 molecules of BI bound in parallel in the junction is more than double the conductance of a single BI monomer by a significant margin. We note that this is different from previous work, both in early model approaches,[25,26] or atomistic calculations and experiments,[27] which reported increased conductance in double-backbone molecules. While in those cases the origin was the spectral properties of two molecular structures coupled to the electrodes through *the same* linkers, here, as we show below, the increased per-molecule conductance is due to more transparent geometries induced by the dimer assembly.

To understand these conductance trends and the source of conductance enhancement in dimer junctions, we turn to DFT atomistic calculations. We use the SIESTA[28] and TRANSIESTA[29] packages including van der Waals interactions in a self-consistent description[30] to calculate the structure and conductance of BI and Im junctions (technical details of the calculations are presented in the SI). We build neutral junctions where BI and Im molecules form chemical bonds to the electrodes through Au trimer structures on the (111) surfaces. Each molecule in the simulations establishes a strong Au-N bond to each electrode. The calculated binding energy of individual molecules at the junction is -2.71 eV (BI) and -2.40 eV (Im) (see Supporting Information Table S2). These values are about double and ~30% larger than amine and pyridine linked molecules, respectively, and are supported experimentally by the relatively longer molecular features observed in 2D histograms in Figure 1a and b than would be expected for similar length amine alkanes, for example.[31,32] This result is consistent with the deprotonation of N atoms in BI and Im, where the charge on the molecule reinforces the binding to gold through image-charge interactions as has been previously shown.[8,12,33]

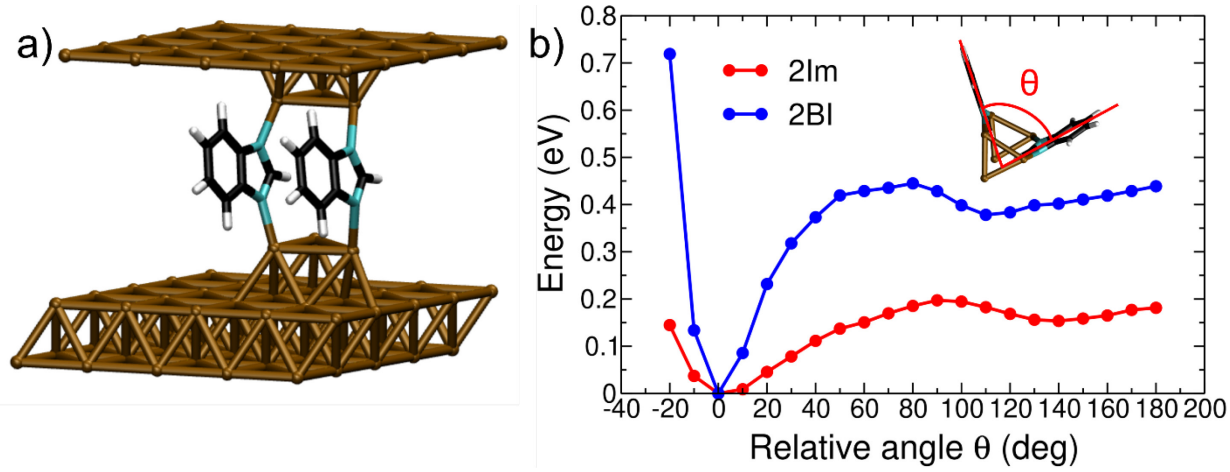

Figure 2. a) Unit cell used in the simulations to probe the angular dependence of the total energy in Im and BI junctions with two molecules. b) Total energy (relative to the minimum value of each species) as a function of the relative angle between both molecules, calculated for two Im (red) and two BI (blue) molecules adsorbed on the same tip structures. The inset illustrates the relative angle θ from a top view of the molecules and tip structures.

We first investigate the energetics of BI and Im dimers at the junction. Since van der Waals distances between conjugated molecules are comparable to the Au-Au nearest-neighbor separation (~3.0 Å), we build junctions where two molecules are bonded to the same tip structures. For this reason, we use trimer motifs in the structure and electron transport simulations. Figure 2a illustrates the unit cell used in the energy profiles, consisting of both molecules bonded to trimer structures and three Au(111) layers. To study the structure of the dimers, we scan the relative angle between both molecules. We constrain the position of all C and N atoms in each molecule such that these atoms can move rigidly but cannot rotate around an axis, leaving the relative angle between the backbones, θ, fixed.[34] H atoms, as well as Au tip atoms, are allowed to move unconstrained.

Figure 2b shows the relative total energy of the junction as a function of θ for BI and Im dimers. Zero energy represents the most stable configuration for each species. In both cases, the most energetically favorable conformation is found when the molecules in the dimer adopt a parallel orientation (θ = 0 deg). There, both conjugated backbones are parallel and π stacking is maximized.[35] At negative values of θ, the molecules are close to each other and repulsion of electron clouds dominate. In the positive range, as θ increases, attractive intermolecular interaction is reduced as the conjugated systems are rotated away from coplanarity and the energy increases.

Fig. S3 shows that van der Waals dispersion interactions are largely responsible for this intermolecular attraction in BI dimers. Both systems exhibit a second, local, minimum at large values of θ. For BI (Im) dimers, this happens at θ = 110 deg (140 deg), and it is around ~0.4 eV (~0.15 eV) less favorable than the parallel arrangement. A fully relaxed geometry optimization, with no constraints, of the antiparallel orientation finds that BI and Im dimers at the junction also exhibit a local minimum in this configuration but in both cases, this is less favorable than the parallel arrangement by 0.26 and 0.05 eV respectively. These relative differences found at the junction are consistent with the values found for gas-phase dimers (see Supporting Information Table S3 and Figure S2).

To summarize, calculations indicate that in BI dimers, the most likely configuration at the junction is overwhelmingly one where the molecules are arranged in parallel. In contrast, in Im dimers the energy profile is less sensitive to the relative angle between Im molecules. We conclude that Im dimer junctions are significantly more likely to explore geometries with large relative angles than BI.

Having established the most likely relative orientations of Im and BI dimers, we now turn to electron transport simulations. We determined the most energetically favorable orientation of single Im and BI molecules at the junction without any constraints and performed electron transport calculations on optimized geometries. Figure 3a compares the calculated transmission spectra of Im and BI junctions. Both spectra exhibit sharp features approximately 0.5 eV below the Fermi level, which correspond to π molecular resonances. In Im, there is a single narrow peak at -0.6 eV while in BI monomer junctions, two features are present at -0.6 eV and at -0.4 eV. The real-space representation of the most transmitting scattering state at -0.4 energy, shown in Figure 3b, reveals that it is derived from a π state delocalized over both the imidazole and benzene rings. However, at the Fermi energy the most transmitting scattering states have in-plane σ symmetry in both Im and BI junctions as shown in Figure 3c and 3d, respectively. In both molecules, this σ resonance peaks is at -1.5 eV, but its coupling at the Fermi energy is overall lower in BI than in Im. The calculated conductance values of Im and BI are $6.4 \times 10^{-2} G_0$ and $4.2 \times 10^{-2} G_0$ respectively, in reasonably good agreement with the experimentally determined values for the G1 peak listed in Table 1.[5,36,37]

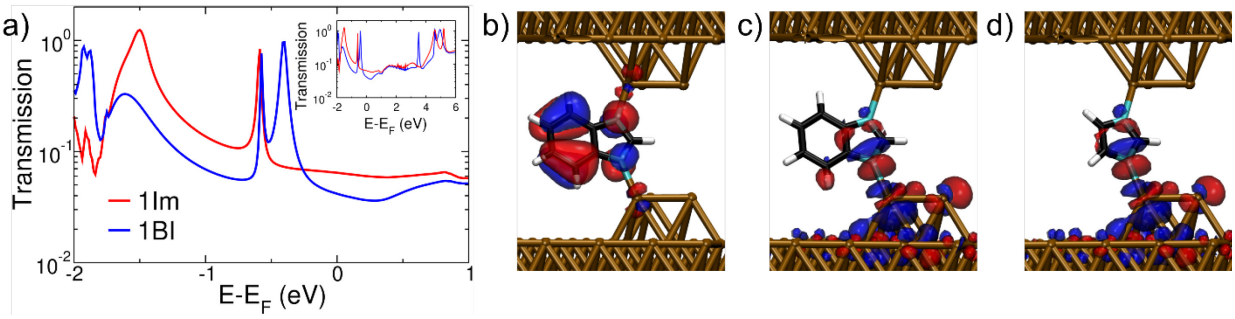

Figure 3. a) Transmission spectra of individual Im and BI molecular junctions. Real-space representation of the most conducting transmission eigenchannel at the center of the Brillouin zone for b) BI at -0.4 eV, c) BI at the Fermi energy, and d) Im at the Fermi energy.

Next, we calculate the conducting properties of Im and BI dimers (2Im and 2BI) to investigate the experimentally determined G2 values. We build junctions with molecular dimers and optimize the interface geometry, where no restrictions are imposed on the geometry of the molecules. Figure 4a shows the computed transmission spectra of 2BI and 2Im in their lowest-energy configuration where both BI and Im molecules are in a parallel orientation. Additional sharp resonances appear near the Fermi level in the occupied part of the spectrum. Their energy and width are different from those of Fig. 3a as a result of enhanced interaction resulting from the small intermolecular distances. In Im dimers, the π resonance closest to the Fermi level is at -0.6 eV. In contrast, in BI dimers this is found at -0.4 eV and is significantly broader, indicative of stronger electronic coupling, yet it does not determine zero-bias conductance.

The most conducting scattering states at the Fermi level, calculated at the center of the Brillouin zone, are shown in Figures 4b (BI dimer) and 4c (Im dimer). The similarity of the nodal patterns indicates that the same σ states are responsible for low-bias transport in all junctions. The calculated conductance values of 2Im and 2BI in their parallel configuration are $14.3 \times 10^{-2} G_0$ and $9.1 \times 10^{-2} G_0$, respectively, which yield G2/G1 ratios of 2.2 for both species when considering the parallel arrangement of molecules in the dimers. This ratio is close to the experimentally determined value of 2.3 for BI but is higher than the one for Im. However, we found previously that non-parallel configurations were energetically accessible for Im and inaccessible in BI at room temperature. We therefore computed the conductance of the Im dimer for other values of θ compatible with an increase in energy of ~2k_BT from the minimum, which all yield lower conductance values: $12.5 \times 10^{-2} G_0$ (θ = -10 deg), $12.3 \times 10^{-2} G_0$ (θ = 10 deg),

and $12.3 \times 10^{-2} G_0$(θ = 20 deg) and all result in G2/G1 ratios of ~1.9. We conclude that when considering accessible conformations for Im dimers, the averaged G2/G1 ratio will be lower than for θ = 0 deg and closer to the measured value. In BI dimers, on the other hand, the parallel orientation is strongly favored over other relative angles and the results of the parallel geometry are therefore representative.

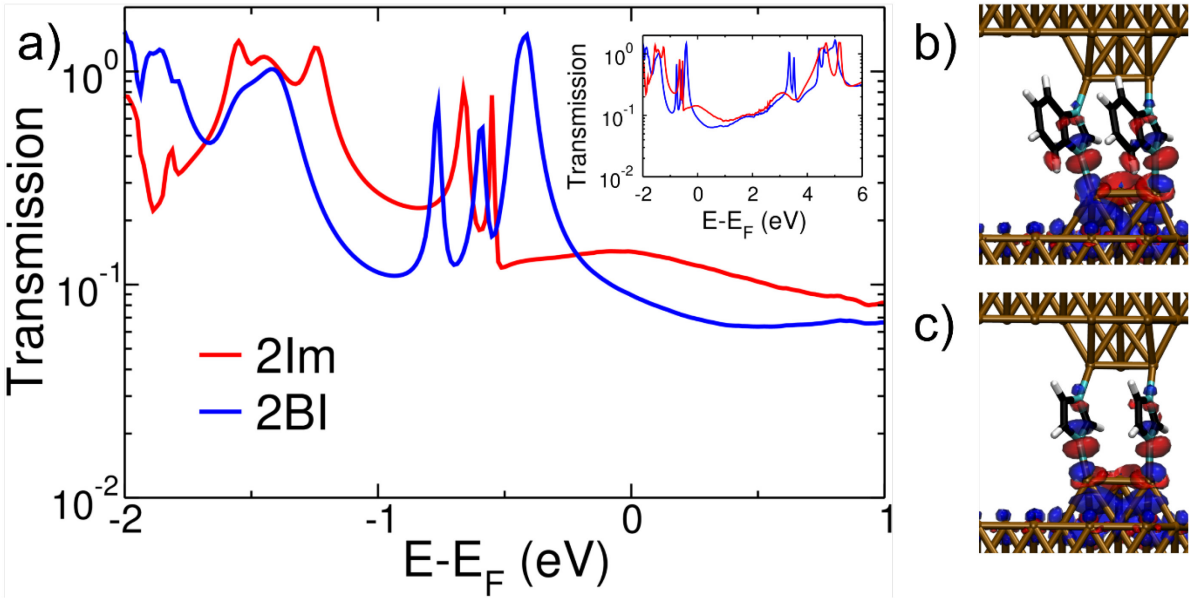

Figure 4. a) Transmission spectra of Im and BI dimers. Real-space representation of the most conducting transmission eigenchannel for b) BI dimers at the Fermi energy, and c) Im dimers at the Fermi energy.

To investigate the origin of the increased conductance of the dimers, we compute individually the transmission of each of each molecule in the geometry that it adopts in the dimer. Starting from the structure of the dimer junction in the parallel conformation, we remove the coordinates of one molecule without changing the coordinates of the remaining atoms in the junction and compute the transmission. The calculated conductance values of BI (Im) molecules, frozen at the geometry adopted in the dimer, are $4.6 \times 10^{-2} G_0$ ($7.5 \times 10^{-2} G_0$) and $4.5 \times 10^{-2} G_0$ ($7.3 \times 10^{-2} G_0$), approximately 10% higher than the value obtained when the geometry of a single BI (Im) molecule is optimized (see Supporting Information Table S4). We find that this stems from changes in the orientation of the molecule with respect to the Au-Au bonds in the tip structures (Fig. S4) when the second molecule is adsorbed forming the dimer. The presence of π

stacking thus restricts each molecule of the dimer to a conformation that is different and more conductive than the conformation it adopts when there is only one molecule in the junction.

Guided by these insights into conductance enhancement mechanisms, we design a molecule which can self-assemble into dimer junctions with increased cooperativity due to intermolecular coupling as in BI, but which retains the high monomer conductance of Im. To do this, we retain the Im core, but substitute it with bulky aromatic or aliphatic moieties which increase the surface area for intermolecular interactions. The histograms and structures of these Im derivatives, 2-phenylimidazole (2PhIm), 2-methylimidazole (2MeIm), are shown in Figure 5a and S6. For comparison, we also measure the conductance of analogous BI derivatives, 2-phenylbenzimidazole (2PhBI), 2-methylbenzimidazole (2MeBI), shown in Figure 5b.

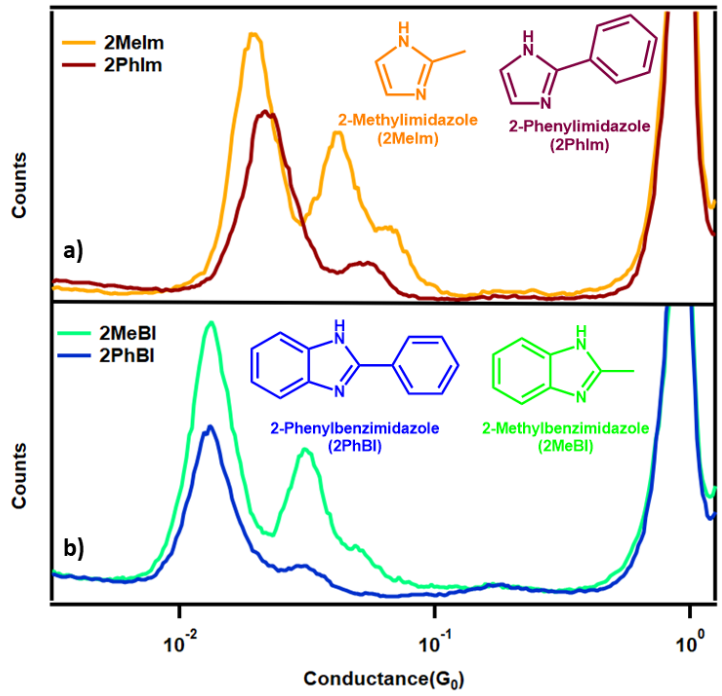

Figure 5. (a) Conductance histograms of 2-methylimidazole (2MeIm) and 2-phenylimidazole (2PhIm). Inset: Chemical structure of 2MeIm and 2PhIm. b) Conductance histograms of 2-phenylbenzimidazole (2PhBI) and 2-methylbenzimidazole (2MeBI). Inset: Chemical structure of 2PhBI and 2MeBI. Both conductance histograms are cut off at 10^{-3} G_0 to focus on the HG region only.

For all four molecules, the HG features of BI and Im are preserved, indicating successful junction formation through the nitrogen atoms as before. The steric bulk of the substituents decreases the amplitude of G2 in all molecules but does not abrogate the formation of dimers in

the junction. The fits to conductance of all BI derivatives are listed in the right column of Table 1. We observe that the G1 and G2 peak positions of 2PhBI and 2MeBI are nearly identical and G2/G1 ratio for these molecules remains ~2.3 as in the BI result. We conclude that substituents alter the probability of observing dimers on atomic-scale contacts as evidenced by lower amplitude peaks, but do not significantly alter the π- π stacking interaction of BI derivatives.

The conductance histograms and fit values in Figure 5a and Table 1 for Im substituted molecules reflect a different pattern. The 2MeIm and 2PhIm display a G2/G1 ratio of 2.21 and 2.38 respectively, which is higher compared to Im, suggesting increased intermolecular stacking interaction in both substituted molecules. For 2MeIm, we note that the electron donating nature of the methyl group increases the electron density on the π system of the Im core and the larger surface area of 2MeIm compared to Im also promotes van der Waals interactions and parallel binding in the junction. Notably, the measured dimer conductance enhancement in 2PhIm is greater than in 2MeIm and approaches the level in BI at G2/G1 ~2.3. The computed energy profile of 2PhIm dimer (Figure S5) shows a steep dependence on the relative angle between the molecules, which is similar to what was observed for BI dimers in Figure 2B. The calculated G2/G1 ratio of 2PhIm dimers is 2.12.

We note that, while the G2/G1 ratio is similar in 2PhIm and BI, the *absolute* conductance of the 2PhIm dimer is 4.94×10^{-2} G_0 compared to 2.64×10^{-2} G_0 for BI. We have succeeded in engineering a self-assembled molecular junction with nearly double the transmission of BI, by leveraging a higher monomer conductance of the Im core and increased intermolecular coupling through aryl substitution which promotes dimers with higher conductance per molecule unit.

To conclude, we demonstrate that BI molecules bridge gold electrodes in parallel, and result in multimer junctions with higher conductance per molecule than monomer BI junctions. We perform detailed theoretical studies to explore the origin of the enhanced conductance effect. Our calculations show that in parallel-stacked BI dimers, the intermolecular binding energy is greater than 20 k_BT. In comparison, Im dimers have a higher degree of conformational freedom to access greater relative stacking angles between molecules. The preferential binding of BI molecules with aligned backbones leads to a binding conformation that is distinct from and more conductive than the conformation adopted by a single molecule in the junction. We demonstrate the potential of harnessing cooperative binding for molecular electronics by designing Im

derivatives that have higher monomer conductance and promote π–π coupling to achieve further conductance enhancement in dimer junctions. This work identifies the potential for π-π driven self-assembly of more transparent molecular circuits and points to new ways of engineering molecular devices by tuning intermolecular interactions.

ASSOCIATED CONTENT

Supporting Information

The supplementary material includes sample preparation procedures, calculation procedures of junction geometry and transmission properties, additional gas phase intermolecular energies of BI, full 1D conductance histograms of substituted BI and Im molecules.

AUTHOR INFORMATION

Corresponding Author

*Maria Kamenetska, orcid.org/ 0000-0002-0390-035X, mkamenet@bu.edu

*Héctor Vázquez: 0000-0002-3865-9922, vazquez@fzu.cz

Author Contributions

The manuscript was written through contributions of all authors. X.P. and E.M. contributed equally. All authors have given approval to the final version of the manuscript.

Funding Sources

This work was supported by the Air Force Office of Scientific Research FA9550-18-S-0002 Young Investigator Research Program, the Operational Programme Research, Development and Education financed by European Structural and Investment Funds and the Czech Ministry of Education, Youth and Sports (Project No. SOLID21 - CZ.02.1.01/0.0/0.0/16_019/0000760). X.P., B.L., and M.K., acknowledge support from the Boston University Photonics Center. Computational resources were supplied by the project "e-Infrastruktura CZ" (e-INFRA LM2018140) provided within the program Projects of Large Research, Development and Innovations Infrastructures

Notes

The authors declare no competing financial interest.

References

1. Aviram, A. & Ratner, M. A. Molecular rectifiers. *Chem. Phys. Lett.* **29**, 277–283 (1974).
2. Perrin, M. L., Burzurí, E. & Van Der Zant, H. S. J. Single-molecule transistors. *Chem. Soc. Rev.* **44**, 902–919 (2015).
3. Su, T. A., Neupane, M., Steigerwald, M. L., Venkataraman, L. & Nuckolls, C. Chemical principles of single-molecule electronics. *Nat. Rev. Mater.* **1**, 1–15 (2016).
4. Sun, L. *et al.* Single-molecule electronics: From chemical design to functional devices. *Chemical Society Reviews* vol. 43 (2014).
5. Evers, F., Korytár, R., Tewari, S. & Van Ruitenbeek, J. M. Advances and challenges in single-molecule electron transport. *Rev. Mod. Phys.* **92**, 35001 (2020).
6. Perrin, M. L. *et al.* Single-molecule functionality in electronic components based on orbital resonances. *Phys. Chem. Chem. Phys.* **22**, 12849–12866 (2020).
7. Wu, S. *et al.* Molecular junctions based on aromatic coupling. *Nat. Nanotechnol.* **3**, 569–574 (2008).
8. Pan, X., Lawson, B., Rustad, A. M. & Kamenetska, M. PH-Activated Single Molecule Conductance and Binding Mechanism of Imidazole on Gold. *Nano Lett.* **20**, 4687–4692 (2020).
9. Skipper, H. E., May, C. V., Rheingold, A. L., Doerrer, L. H. & Kamenetska, M. Hard–Soft Chemistry Design Principles for Predictive Assembly of Single Molecule-Metal Junctions. *J. Am. Chem. Soc.* **143**, 16439–16447 (2021).
10. Wu, C. *et al.* In situ formation of H-bonding imidazole chains in break-junction experiments. *Nanoscale* **12**, 7914–7920 (2020).
11. Pan, X., Qian, C., Chow, A., Wang, L. & Kamenetska, M. Atomically precise binding conformations of adenine and its variants on gold using single molecule conductance signatures. *J. Chem. Phys.* **157**, 234201 (2022).
12. Li, S., Jiang, Y., Wang, Y. & Hou, S. The Formation and Conducting Mechanism of Imidazole-Gold Molecular Junctions. *ChemistrySelect* **6**, 2959–2965 (2021).
13. Solomon, G. C., Vura-Weis, J., Herrmann, C., Wasielewski, M. R. & Ratner, M. A. Understanding coherent transport through π-Stacked systems upon spatial dislocation. *J. Phys. Chem. B* **114**, 14735–14744 (2010).
14. Li, X. *et al.* Structure-Independent Conductance of Thiophene-Based Single-Stacking Junctions. *Angew. Chemie Int. Ed.* **59**, 3280–3286 (2020).
15. Zhang, C. *et al.* Enhanced π-π Stacking between Dipole-Bearing Single Molecules Revealed by Conductance Measurement. *J. Am. Chem. Soc.* **145**, 1617–1630 (2023).
16. Martín, S. *et al.* Identifying diversity in nanoscale electrical break junctions. *J. Am. Chem.*

Soc. **132**, 9157–9164 (2010).

17. Frisenda, R., Janssen, V. A. E. C., Grozema, F. C., Van Der Zant, H. S. J. & Renaud, N. Mechanically controlled quantum interference in individual Ï-stacked dimers. *Nat. Chem.* **8**, 1099–1104 (2016).

18. González, M. T. *et al.* Break-junction experiments on acetyl-protected conjugated dithiols under different environmental conditions. *J. Phys. Chem. C* **115**, 17973–17978 (2011).

19. Reznikova, K. *et al.* Substitution Pattern Controlled Quantum Interference in [2.2]Paracyclophane-Based Single-Molecule Junctions. *J. Am. Chem. Soc.* **143**, 13944–13951 (2021).

20. Xu, B. & Tao, N. J. Measurement of Single-Molecule Resistance by Repeated Formation of Molecular Junctions. *Science (80-.).* **301**, 1221–1223 (2003).

21. Venkataraman, L. *et al.* Single-molecule circuits with well-defined molecular conductance. *Nano Lett.* **6**, 458–462 (2006).

22. McNeely, J., Miller, N., Pan, X., Lawson, B. & Kamenetska, M. Angstrom-Scale Ruler Using Single Molecule Conductance Signatures. *J. Phys. Chem. C* **124**, 13427–13433 (2020).

23. Kamenetska, M. *et al.* Formation and evolution of single-molecule junctions. *Phys. Rev. Lett.* **102**, 2–5 (2009).

24. Miao, Z. *et al.* Charge Transport Across Dynamic Covalent Chemical Bridges. *Nano Lett.* **22**, 8331–8338 (2022).

25. Sautet, P. & Joachim, C. Electronic interference produced by a benzene embedded in a polyacetylene chain. *Chem. Phys. Lett.* **153**, 511–516 (1988).

26. Magoga, M. & Joachim, C. Conductance of molecular wires connected or bonded in parallel. *Phys. Rev. B* **59**, 16011–16021 (1999).

27. Vazquez, H. *et al.* Probing the conductance superposition law in single-molecule circuits with parallel paths. *Nat. Nanotechnol.* **7**, 663–667 (2012).

28. Soler, J. M. *et al.* The SIESTA method for ab initio order-Nmaterials simulation. *J. Phys. Condens. Matter* **14**, 2745 (2002).

29. Papior, N., Lorente, N., Frederiksen, T., García, A. & Brandbyge, M. Improvements on non-equilibrium and transport Green function techniques: The next-generation transiesta. *Comput. Phys. Commun.* **212**, 8–24 (2017).

30. Román-Pérez, G. & Soler, J. M. Efficient implementation of a van der waals density functional: Application to double-wall carbon nanotubes. *Phys. Rev. Lett.* **103**, 096102 (2009).

31. Lawson, B., Zahl, P., Hybertsen, M. S. & Kamenetska, M. Formation and Evolution of Metallocene Single-Molecule Circuits with Direct Gold-π Links. *J. Am. Chem. Soc.* **144**, 6504–6515 (2022).

32. Yoshida, K. *et al.* Correlation of breaking forces, conductances and geometries of molecular junctions. *Sci. Rep.* **5**, 9002 (2015).

33. Vladyka, A. *et al.* In-situ formation of one-dimensional coordination polymers in molecular junctions. *Nat. Commun.* **10**, 1–9 (2019).

34. Doud, E. A. *et al.* Cyclopropenylidenes as Strong Carbene Anchoring Groups on Au Surfaces. *J. Am. Chem. Soc.* **142**, (2020).

35. Brédas, J. L., Calbert, J. P., Da Silva Filho, D. A. & Cornil, J. Organic semiconductors: A theoretical characterization of the basic parameters governing charge transport. *Proc. Natl. Acad. Sci. U. S. A.* **99**, (2002).

36. Refaely-Abramson, S., Liu, Z. F., Bruneval, F. & Neaton, J. B. First-Principles Approach to the Conductance of Covalently Bound Molecular Junctions. *J. Phys. Chem. C* **123**, (2019).

37. Montes, E. & Vázquez, H. Calculation of Energy Level Alignment and Interface Electronic Structure in Molecular Junctions beyond DFT. *J. Phys. Chem. C* **125**, (2021).

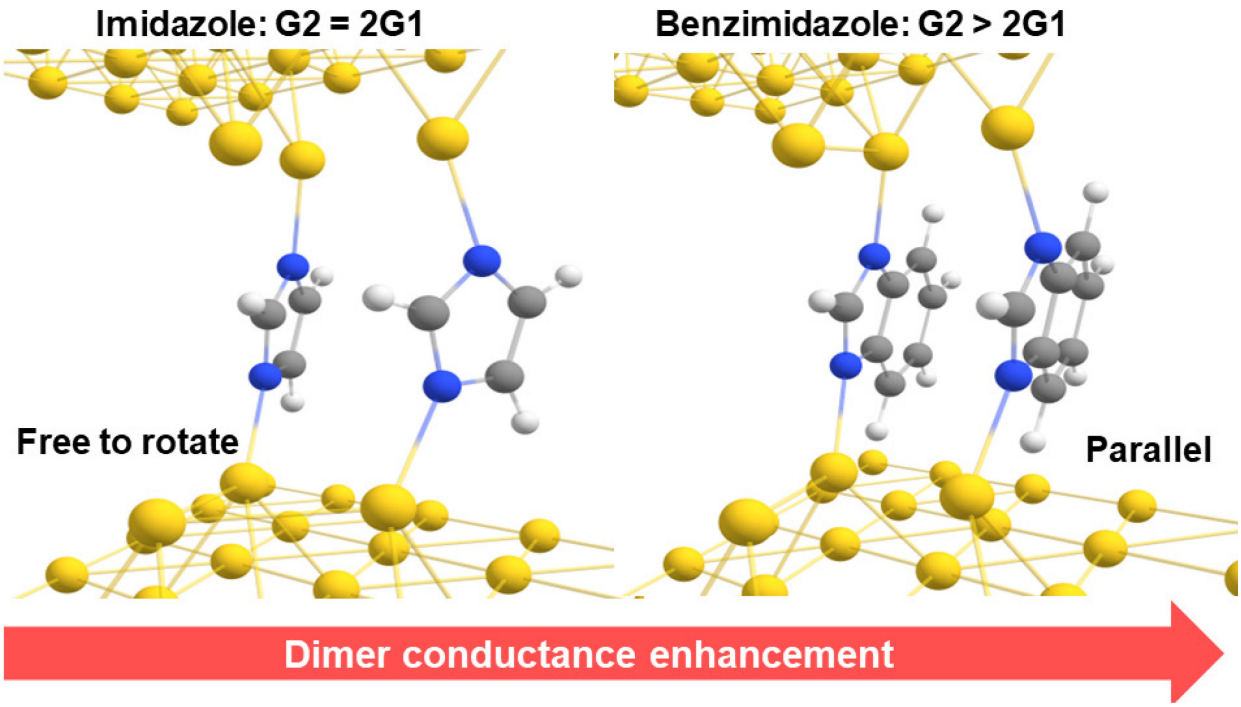

TOC